

## THE APPLICATION OF PROTONS TO COMPUTED TOMOGRAPHY\*

K.M. Hanson, J.N. Bradbury, T.M. Cannon, R.L. Hutson,  
D.B. Laubacher,<sup>†</sup> R. Macek, M.A. Paciotti and C.A. Taylor<sup>††</sup>University of California  
Los Alamos Scientific Laboratory  
Los Alamos, NM 87545

The results of an experiment are presented which verify previous calculations that indicate protons can be used to obtain Computed Tomographic (CT) reconstructions with a considerably lower dose than that required by x rays for reconstructions of the same quality. Furthermore, the use of protons virtually eliminates the beam hardening artifacts encountered in x-ray CT scanners. A CT density reconstruction of a 30 cm diameter phantom obtained with 240 MeV protons at LAMPF is compared with a reconstruction of the same phantom obtained with a commercial x-ray scanner. The advantages and disadvantages of this application of protons are discussed.

Introduction

It has been realized for some time that the energy loss characteristics of protons and other heavy charged particles could be used to obtain radiographs. At first, the major interest in this new modality centered on its inherently higher contrast compared with x rays.<sup>1</sup> Calculations have shown that this modality also provides better integrated density, or pathlength, information per unit dose for thick biological specimens than does the conventional x-ray modality.<sup>2-5</sup> This latter advantage could be important in the application of heavy charged particles to medical computed tomography (CT). Present day commercial x-ray CT units deliver skin doses ranging from about 1 rad to well over 10 rads.<sup>5</sup> Furthermore, the resolving power attainable with protons is comparable to that achieved in the x-ray units where the limitation appears to be related to the maximum allowable patient dose.

Summary of Calculations

In the CT method, the two-dimensional density distribution in a plane through a specimen is reconstructed from a series of one-dimensional integrated density distributions taken through that section at various angles. The proton CT technique obtains the integrated density distributions, or projections, by measuring the energy lost by protons which traverse the specimen. The uncertainty in the integrated density is the result of energy loss straggling. Detailed calculations<sup>5</sup> have been performed by one of the authors (KMH) to compare the proton and x-ray doses required to produce reconstructions of identical density resolution. In the proton calculation, it was assumed that the uncertainty in the pathlength for one proton is given by the range straggling.<sup>7</sup> A correction was made for the fraction of incident protons which undergo nuclear interaction rendering them unusable. The x-ray dose was calculated using the energy absorption coefficient and the backscatter factor. Both proton and x-ray depth distributions were taken into account assuming a series of scans with a full 360° range of projection angles. A

mono-energetic x-ray beam was assumed. The calculations indicate that at the optimum x-ray and proton energies protons could provide the same density resolution as monochromatic x rays with a reduction of the surface dose by a factor of 3.9 for a 20 cm diameter specimen and a factor of 8.2 for a 30 cm specimen.

The spatial resolution achievable with protons is limited by multiple Coulomb scattering which leads to the spatial spreading of a pencil beam as it passes through the specimen. A Monte Carlo program was used to determine the magnitude of this spatial spreading. The program used a Gaussian approximation to the Molière distribution<sup>8</sup> including the contribution from scattering from the atomic electrons<sup>9</sup> and incorporated the proton energy loss. As shown in Figure 1, a 230 MeV pencil proton beam will spread to a width of 4.4 mm (FWHM) in the middle of a 30 cm diameter tissue specimen and to a width of 14 mm at exit. The spatial resolution obtained in commercial scanners is approximately 2 mm<sup>5</sup> indicating a need to improve the proton spatial resolution. This may be accomplished by measuring the position of the protons as they exit from the specimen. As depicted in Figure 1, this method results in good spatial resolution at entrance and at exit with the worst resolution, about 3.4 mm, occurring near the center of the specimen. Another possible approach uses heavier charged particles such as alpha particles.<sup>2-4</sup>

Apparatus

An experiment was performed on the P<sup>3</sup> West channel at LAMPF to demonstrate the feasibility of obtaining high quality proton CT reconstructions. The experimental layout is shown schematically in Figure 2. The experimental method determines the residual energy of a

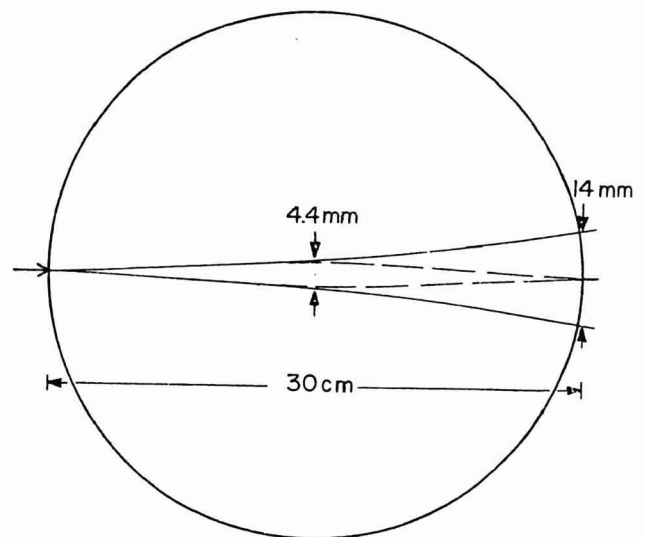


Figure 1

Spreading (FWHM) of a 230 MeV proton beam with measurement of exit position, dashed line, and without, solid line.

\* Work supported by funds from the U.S. Energy Research and Development Administration.

<sup>†</sup> Permanent address: Purdue University, West Lafayette, IN 47906

<sup>††</sup> Permanent address: Norfolk State College, Norfolk, VA

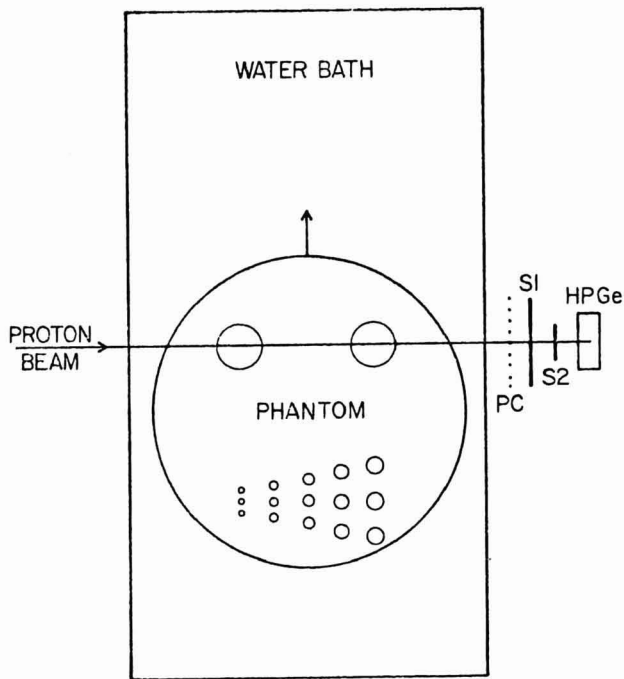


Figure 2

Plan view of experimental setup. During the CT scans the phantom was translated and rotated while the proton beam remained stationary.

nearly monoenergetic proton beam after it had passed through a plastic phantom. The mean residual energy was used to determine the mean residual range which is a measure of the amount of material traversed by the beam.

A specially developed tune of the  $P^3$  channel provided a proton beam with a 0.2% momentum bite. The beam spot was about 1.6 mm (FWHM) wide and 3 mm high. The beam divergence was typically 14 mrad (FWHM).

The horizontal beam waist was typically positioned about 10 cm into the water bath. The residual energy of each proton was measured with a hyperpure germanium (HPGe) detector supplied by the detector group at the Lawrence Berkeley Laboratory. The HPGe detector had a diameter of 3.3 cm and a thickness of 1.25 cm. Protons with energies of up to 70 MeV stop in this detector. The event trigger was obtained from the two 3 mm thick scintillation counters, S1 and S2. Counter S2, with an active diameter of 2 cm, restricted the events to the central region of the HPGe detector to avoid edge effects. A helical delay-line readout proportional chamber (PC) was used to measure the horizontal deflection of each proton at the exit of the water bath. During the measurements the phantom was moved under computer control through the water bath across the beam. At the end of each traverse, the phantom was rotated by computer command before a new traverse was begun. The position reproducibilities of the scanning servomechanisms were  $\pm 0.2$  mm in translation and  $\pm 0.1$  degree in rotation.

Besides the water bath and the phantom, the significant material in the beam before the HPGe detector consisted of 0.32 cm plexiglas and 0.32 cm aluminum in the walls of the water tub, 0.64 cm of plastic scintillator in S1 and S2, and 0.73 g/cm<sup>2</sup> of polyethylene placed between PC and S1 to adjust the mean residual energy detected in HPGe.

Two ADC's were run in parallel measuring the HPGe pulse height and the proton position at PC. Event

pileup was eliminated through the use of fast logic. The event data were read into a PDP-11/45 computer and put on magnetic tape for later analysis. The use of Nuclear Enterprises 9060 buffered CAMAC analog-to-digital converters (ADC) permitted an average data acquisition rate of 740 events per second with about 50% electronic deadtime at a LAMPF beam duty factor of 6%.

### Experimental Results

Figure 3 shows a typical residual energy distribution measured by the HPGe detector for an initial proton energy of 240 MeV. At the mean energy of the fitted Gaussian distribution of 36 MeV the r.m.s. width of the residual energy distribution predicted by range

straggling in water is 6.6 MeV.<sup>10</sup> The fitted width of 6.7 MeV is in good agreement with this value. Thus the fluctuations in the residual energy are dominated by the energy loss straggling in the 30.5 cm water bath.

The experimental method was shown to have sufficient stability to produce high quality tomograms. A 210 MeV proton beam was used with a 25.4 cm thick polyethylene degrader in place of the water bath. The residual proton energy was 45 MeV with an r.m.s. width of 4.5 MeV caused by straggling in the polyethylene. Approximately 40,000 events were accumulated in each run to reduce the statistical error in the mean residual energy to 23 keV. In a series of such runs the r.m.s. deviation in the residual energy was found to be 41 keV indicating the presence of drifts in the stability of the system. The measured energy drifts imply the r.m.s. drift in the mean momentum of the incident beam is less than 0.004%.

The pathlength sensitivity of the system was demonstrated by placing a single sheet of paper in front of the polyethylene. The resulting 180 keV shift of the residual energy, clearly visible in Figure 4, corresponds to the addition of 0.013 g/cm<sup>2</sup> of polyethylene, or less than 0.06% of the original material thickness.

A CT scan was performed on a 29.4 cm diameter plastic phantom which was designed to permit a direct comparison of proton and x-ray reconstructions. The translation scans were made in 1.25 mm steps. Approximately 675 events were taken at each position in a period of 0.9 sec. Data taking was suspended for 0.2 sec to allow the scanner to reach the next position. The phantom was overscanned by 1.5 cm on each side to permit water calibrations at the end points of each projection. Three hundred and sixty projections were taken with 1 deg increments between each. In all 62.5 million events were obtained in a total running time of 45 hours. Measurements indicated that due to nuclear scattering in the phantom 54% of the incident protons reached S1. Fifty-two percent of the protons reaching S1 fell

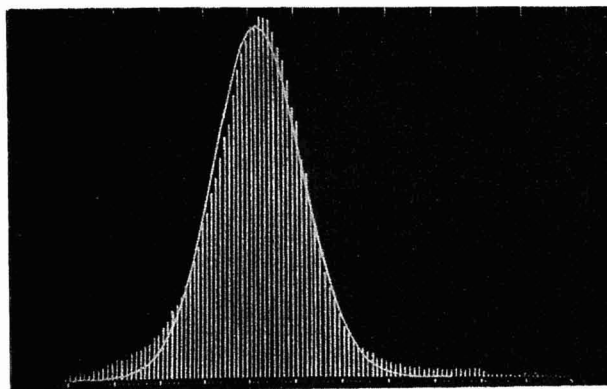


Figure 3

HPGe energy spectrum for 30.5 cm water bath and initial proton energy of 240 MeV. The width of the energy peak is dominated by energy straggling in the water bath.

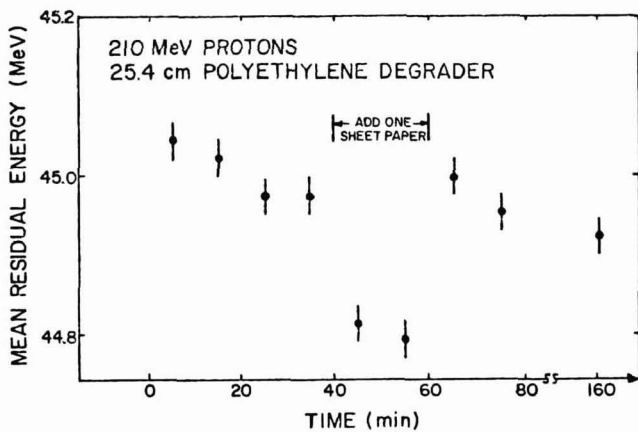


Figure 4

The stability of the mean residual energy detected by the HPGe detector is demonstrated in a series of runs, each containing about 40,000 events. The effect of the addition of a single sheet of paper is readily apparent.

inside the 2 cm diameter of S2 and hence were eligible to produce an event trigger. The average dose, calculated for a 1 cm thick slice in a series of scans in order to compare it with typical x-ray scanner geometries, is 0.6 rad. This dose is based on the number of incident protons needed to produce 62.5 million good events and takes into account the above mentioned geometrical attenuation factors. It does not include electronic, computer and scanner deadtimes experienced in our specific experimental setup. In an apparatus designed to reduce dose to a patient, these factors can be significantly reduced.

The residual energy distributions measured by the HPGe detector were fit by a Gaussian function as shown in Figure 3. The mean residual energy was then expressed in terms of residual range using a power law relationship. The calibration of the residual range was accomplished by scanning a teflon step wedge. The residual range in the water bath was determined at the beginning and end of each traverse. These residual ranges were subtracted from the intermediate scan values using linear interpolation, thus expressing the scan data in terms of residual range relative to water. At each scan point the data were binned according to the proton position in PC into eight 2 mm wide bins. After fitting these eight energy distributions, eight residual ranges were calculated.

A filtered backprojections algorithm was used to produce a reconstruction with 1.25 mm x 1.25 mm pixel size. A Hanning filter that dropped to 0.5 at one half the Nyquist frequency was incorporated. The exit position information contained in the eight residual ranges at each scanner position was included by backprojecting along a straight line which approximated the most probable curved path followed by the protons reaching the respective bins in PC.

The proton CT reconstruction of the 29 cm phantom is displayed in Figure 5. The high and low contrast resolution sections of the phantom have essentially the same chemical composition as the background material, polyethylene of normal density,  $0.920 \text{ g/cm}^3$ . The high contrast sections consist of polyurethane filled holes 1 to 3 mm diameter in 0.25 mm steps with spacing equal to the diameter. The low contrast section consists of 3.2, 4.8, 6.4, 9.5 and 1.27 mm diameter holes filled with high density polyethylene plugs. The density difference and hence contrast relative to the background is  $(1.8 \pm 0.2)\%$ . The resolving power of the proton

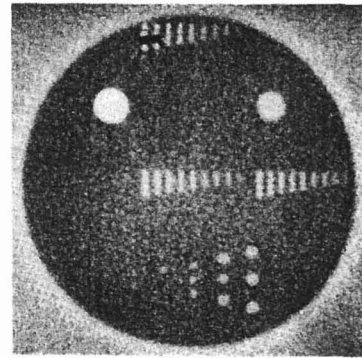


Figure 5

Proton CT reconstruction of the 29 cm phantom obtained at an equivalent average dose of 0.6 rads in a 1 cm thick slice.

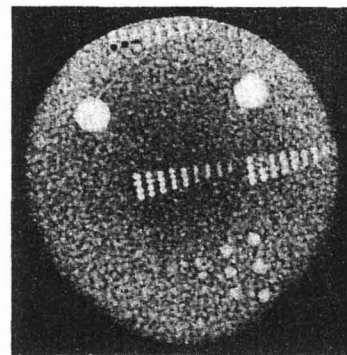


Figure 6

EMI 5005 reconstruction of the 29 cm phantom obtained at an equivalent average dose of 2.2 rads in a 1 cm thick slice.

reconstruction is about 2.25 mm. The low contrast resolution is between the third and fourth largest holes, say 5.8 mm diameter at 1.8% contrast. The r.m.s. noise in the proton reconstruction with the filtering described above is 0.3%.

For comparison, a CT scan of the same phantom taken on an EMI 5005 scanner without a water bath is shown in Figure 6. The 320 x 320 data matrix from the EMI scan has been spatially filtered to the same extent as the proton image and subsequently displayed in a 256 x 256 format. The low contrast resolution is not quite as good as the third row of holes, namely about 7.4 mm diameter at 1.8% contrast. The EMI scan was actually taken at 90 kV at slow speed which results in an r.m.s. noise about 25% larger than that found in a normal 20 sec scan. The average dose in such a normal scan is 2.2 rad with a peak skin dose of 5.5 rad for a series of scans with 1 cm steps.<sup>6</sup> The resolving power of the EMI scan when displayed in the magnified format available on the scanner console is 1.5 mm. Note the center region of the EMI image is darker than the outside. This beam hardening artifact is completely absent in the proton reconstruction. The ratio of low contrast resolutions observed in Figure 6 to that in

Figure 5 is 1.28. It is nearly the same as the ratio of the r.m.s. noise level in Figure 6 to that in a normal EMI 5005 20 sec scan. We conclude that the normal EMI scan produces an image with approximately the same density resolution as our proton scan. The net average dose advantage of the proton scan over the EMI x-ray scan is thus  $2.2/0.6 = 3.7$ . This agrees well with the calculated dose advantage when one takes into account that in the present experiment half the protons reaching S1 were not used because they fell outside the 2 cm circle in S2.

#### Discussion

We have demonstrated that the application of protons to computed tomography can result in a significant dose advantage relative to x rays. Thus, at the same dose as is delivered by contemporary commercial x-ray scanners, a proton scanner could produce reconstructions with a factor of 2 or more improvement in density resolution. Whether such an improvement can result in significantly better diagnoses of human disease is an open question which can only be answered by the implementation of a proton scanner in a clinical situation.

The advantages of proton over x-ray CT are as follows:

- a. lower dose for a given density resolution
- b. lack of beam hardening artifacts
- c. fast scans may be possible since the number of protons required (about  $10^8$ ) can be easily supplied in a very short time interval.

The disadvantages of protons are:

- a. accelerators which supply protons of sufficient energy are considerably more complicated, bulky and costly than x ray sources.
- b. delivery of proton beam to a supine patient is more difficult than for x rays, but not impossible.
- c. spatial resolution of proton scans is limited by multiple Coulomb scattering. Use of heavy ions instead of protons may alleviate this problem.
- d. since there are no huge Z effects in proton stopping power as there are in x-ray attenua-

tion, the important diagnostic use of contrast agents is precluded.

#### Acknowledgements

The authors wish to acknowledge Ann Aldridge for her part in designing the special beam tune, David Lee for his assistance with the proportional chambers and Oliver Rivera for his assistance in setting up the experiment. We are indebted to Douglas Boyd for scanning our phantom with the EMI scanner and to Peter Berardo and Sandra Zink for transcribing the magnetic tape from that machine.

#### References

1. A.M. Koehler, Science 160, 303-304 (1968).
2. E.V. Benton, R.P. Henke, C.A. Tobias and M.P. Coutz, Report LBL-2887, August 1975.
3. R.H. Huesman, A.H. Rosenfeld and F.T. Solnitz, Report LBL-3040, September 1975.
4. T.F. Budinger et al., Proc. of Image Processing for 2-D and 3-D Reconstruction from Projections, Stanford, CA, August 4-7, 1975.
5. K.M. Hanson, "Comparison between proton and x-ray axial tomography", presented at Int. Symp on Computer assisted Tomography in Nontumoral Diseases of the Brain, Spinal Cord and Eye, October 1976 and to be published.
6. D.P. Boyd, A.R. Margulis and M. Korobin, to be published in Proc. S.P.I.E., Appli. of Op. Inst. in Medicine VI, 1977.
7. R.M. Sternheimer, Phys. Rev. 117, 485-488 (1968).
8. V.G. Moliere, Z. Naturforschg. 3a, 78-95 (1948).
9. U. Fano, Phys. Rev. 93, 117-120 (1954).
10. J.F. Janni, Air Force Weapons Lab. Technical Report AFWL-TR-65-150 (1966).